



# Multi metallic electro-catalyst design for enhanced oxygen evolution reaction: Immobilizing MnFe nanoparticles on ZIF-67-decorated graphene oxide

Zhwan Naghshbandi <sup>a,d</sup>, Kayvan Moradi <sup>c</sup>, Abdollah Salimi <sup>a,b,\*</sup>, Mohammad Gholinejad <sup>d</sup>, Ali Feizabadi <sup>e</sup>

<sup>a</sup> Department of Chemistry, University of Kurdistan, Sanandaj 66177-15175, Iran

<sup>b</sup> Research Center for Nanotechnology, University of Kurdistan, Sanandaj 66177-15175, Iran

<sup>c</sup> Department of Chemistry, Nanoscience Center, University of Jyväskylä, P.O. Box 35, Jyväskylä FI-40014, Finland

<sup>d</sup> Department of Chemistry, Institute for Advanced Studies in Basic Sciences (IASBS), P.O. Box 45195-1159, Gavazang, Zanjan 45137-66731, Iran

<sup>e</sup> Department of Chemistry, University of Western Ontario, London, ON, Canada

## ARTICLE INFO

### Keywords:

Oxygen evolution reaction  
Multimetallic electrocatalyst  
MnFe nanoparticles  
Zeolitic imidazolate framework-67-decorated  
graphene oxide

## ABSTRACT

The advancement of large-scale hydrogen production and its application via electrocatalytic water splitting heavily relies on progress in developing highly active inexpensive, and efficient electrocatalysts for oxygen evolution reactions (OER), which continues to pose a significant challenge. Herein, we prepare GO@ZIF-67@MnFe with embedded iron (Fe) and manganese (Mn) nanoparticles on graphene oxide (GO) decorated with a zeolitic imidazolate framework (ZIF-67) using a facile and cost-effective method. The as-prepared GO@ZIF-67@MnFe catalyst exhibits remarkable electrocatalytic activity with a low overpotential of only 236 mV at the current density of 10 mA cm<sup>-2</sup>, a small Tafel slope of 55.7 mV dec<sup>-1</sup>, and robust durability in 1.0 M KOH electrolyte. Additionally, we conduct a systematic study to investigate the electrocatalytic OER activity of ZIF-67, ZIF-67@Mn, ZIF-67@Fe, and ZIF-67@MnFe using density functional theory (DFT) calculations. The experimental and DFT calculation results suggest that the introduction of Fe and Mn to ZIF-67 improves OER performance by reducing the activation energy barrier and accelerating kinetics. This study presents a promising strategy and rational design methodology for the developing multi-metallic catalysts utilizing ZIF derivatives for water splitting.

## 1. Introduction

The increasing concerns about the depletion of fossil fuels, energy crisis and environmental problems have prompted the search for sustainable and efficient energy storage and conversion technologies, with hydrogen production being a promising alternative due to its abundance, high energy density, low molecular weight, and clean nature [1–6]. The oxygen evolution reaction (OER) is a pivotal process in hydrogen production, but it is kinetically sluggish and requires efficient catalysts for advancement. While noble-metal catalysts such as RuO<sub>2</sub> and IrO<sub>2</sub> are ideal for OER, their high cost and limited availability present challenges for large-scale applications [7–10]. Therefore, the persistent research challenge lies in the development of cost-effective, highly efficient, and durable OER catalysts. To achieve this, non-noble

transition metals such as cobalt, nickel, copper, iron, and manganese have been widely investigated as potential substitutes for improving OER catalytic performance. For example, cobalt-based bimetallic phosphide ultrathin nanosheets (CoM-P-NS, M= Ni, Mn, Cu, Zn) [11], Co/Ni dual sites immobilized N-doped porous Janus-like carbon frameworks [12], WCoFe<sub>0.3</sub>-CNF [13], CoFe/Co-bamboo fibres [14], and Co<sub>2</sub>Mo<sub>3</sub>O<sub>8</sub> [15] have been explored as excellent alternatives to costly RuO<sub>2</sub> and IrO<sub>2</sub> materials.

Furthermore, several promising materials have been explored for catalyzing OER, including metal oxides, perovskites, and metal-organic frameworks (MOFs). Among these, MOFs have emerged as a promising class of materials due to their tunable structures and unique properties, including low density, high surface area, permanent porosity, abundant active sites, and chemical stability. Zeolitic imidazolate frameworks

\* Corresponding author at: Department of Chemistry, University of Kurdistan, Sanandaj 66177-15175, Iran.

E-mail address: [absalimi@uok.ac.ir](mailto:absalimi@uok.ac.ir) (A. Salimi).

(ZIFs) are a specific classification of MOFs that have exhibited utility not only in the realm of catalysis but also in a plethora of other applications, including sensors, gas storage, and drug delivery [16–20]. ZIFs are constructed by coordinating a tetrahedral metal cation (such as Zn or Co) and an imidazole ligand (Im), forming an M-Im-M angle of ~145° [21–25].

There has been significant interest in the application of ZIFs and their derivatives as electrocatalysts for OER and as host matrices for metal nanoparticles in electrocatalysis. ZIF-67, in particular, has been extensively studied due to its various morphologies, including rhombic dodecahedron (T-ZIF-67), flower-like (M-ZIF-67), and hollow spherical (H-ZIF-67), with M-ZIF-67 being identified as a highly efficient catalyst for OER [26]. Notably, several other ZIF-based catalysts for OER have also been reported, such as cobalt nanoparticles enclosed within nitrogen-doped carbon nanotubes and grafted carbon nanosheets (LDH-R@Co(v-Zn)-NCNTs), which were synthesized by Yang and co-workers and demonstrated efficient catalytic activity for OER [27]. Similarly, Ren et al. achieved exceptional catalytic activity and stability for OER by designing Co-NC (Carbon Network)@CNTs through the calcination of ZIF-67@CNTs composites [28]. Furthermore, CoN-C/Co@CC, Co-CoO@NSC (nanoparticles encapsulated in N, S co-doped carbon shells), Fe-Co<sub>1.11</sub>Te<sub>2</sub>@NCNTF (nitrogen-doped carbon nanotube frameworks), and other ZIF-based catalysts have also been explored for OER catalysis [29–31].

In recent years, multi-metallic catalysts have been identified as exhibiting superior catalytic activity than monometallic catalysts due to synergistic intermetallic interaction. Therefore, many multi-metallic materials have been applied as catalysts for water splitting in recent years. For instance, WCoFe<sub>0.3</sub>-CNF [13], Co<sub>2</sub>P/Ni<sub>2</sub>P-x%Mo [27], Fe/Co/Zn@C-NCNFS-800 (co-doped carbon nanofibers) [32], and CoP@FeNiP/NF [33] have been designed for this purpose. In addition to these catalysts, graphene oxide (GO) has also attracted considerable attention due to its remarkable properties, including high electrical and thermal conductivity, great specific surface area, extraordinary electron transport capabilities, and high mechanical strength. As a 2D *sp*<sup>2</sup>-hybridized carbon nanosheet, graphene oxide (GO) has been employed in various applications, including water splitting [34], supercapacitors [35], energy storage [36], sensors [37], and biotechnology [38].

In this study, we present a facile and cost-effective procedure for the synthesis of ZIF-67 arrays grown on the surface of GO, followed by embedding bimetallic nanoparticles (Fe and Mn) in GO@ZIF-67 (**Scheme 1**). The resulting electrocatalyst GO@ZIF-67@MnFe exhibited superior catalytic activity for OER in 1.0 M KOH alkaline electrolyte. Notably, the GO@ZIF-67@MnFe electrode with an Mn:Fe ratio of 1:1 outperformed other compositions, including GO@ZIF-67@MnFe (Fe: Mn, 1:2 and 2:1), GO@ZIF-67@Mn, GO@ZIF-67@Fe and GO@ZIF-67. The excellent electrocatalytic performance of the GO@ZIF-67@MnFe electrode was attributed to the synergy effect between GO, ZIF-67, and MnFe, which led to an early onset at 1.43 V, an overpotential of 236 mV at a current density of 10 mA cm<sup>-2</sup>, a Tafel slope of 55.7 mV dec<sup>-1</sup>, and strong durability of 24 h. The synergistic effects between Fe, Mn, Co and graphene oxide led to that catalytic activity in OER being better than in the previously reported literature [39–41], in which a low amount of Mn and Fe in the surface of GO@ZIF-67 increased the catalytic activity. Furthermore, we utilized density functional theory (DFT) calculations to demonstrate the advantages of trimetallic zeolitic imidazolate framework heterostructures compared to single and dual metallic systems for OER performance. These findings offer a novel approach to the design and production of catalysts based on ZIFs, demonstrating their utilization in OER applications.

## 2. Experimental

### 2.1. Materials and characterizations

The chemicals used in this study, including flake graphite, potassium

permanganate (KMnO<sub>4</sub>), Co (OAc)<sub>2</sub>·4H<sub>2</sub>O, 2-methylimidazole, Fe (NO<sub>3</sub>)<sub>3</sub>·9H<sub>2</sub>O, MnSO<sub>4</sub>·H<sub>2</sub>O, potassium hydroxide (KOH) and Nafion were purchased from reputable sources such as Sigma-Aldrich, Acros, and Merck Millipore-Sigma, and were used without further purification. Morphological characterization was performed employing field-emission scanning electron microscopy (FE-SEM MIRA3 FEG-SEM, Tescan, Czech Republic) and transmission electron microscopy (TEM, EM 208S). X-ray diffraction (XRD) measurements were taken using a D-500 diffractometer equipped with a Cu K $\alpha$  radiation source ( $\lambda = 0.15,418$  nm). X-ray photoelectron spectroscopy (XPS) data were collected using a BESTEC (EA 10, Al-K $\alpha = 1486.6$  eV) photoelectron spectrometer. Electrochemical experiments were evaluated on a computer-controlled m-Autolab modular electrochemical system (Eco Chemie Ultecht, The Netherlands), driven with GPS software (Eco Chemie).

### 2.2. Preparation of GO@ZIF-67

Using the improved Hummer method GO was prepared from flake graphite [42]. In a typical procedure, 28 mg of GO were dispersed in 20 mL of methanol, followed by adding of 1 mmol of Co (OAc)<sub>2</sub>·4H<sub>2</sub>O to the solution. Next, a solution of 2-methylimidazole (12 mmol) in 10 mL methanol was added with vigorous stirring for 24 h at room temperature. The resulting product was centrifuged, washed thoroughly with methanol, and dried at 60 °C in an oven.

### 2.3. Preparation of GO@ZIF-67@MnFe

In the next step, 22 mg of GO@ZIF-67 was dispersed in 20 mL of methanol. Fe (NO<sub>3</sub>)<sub>3</sub>·9H<sub>2</sub>O (0.027 mmol, 11 mg) and MnSO<sub>4</sub>·H<sub>2</sub>O (0.065 mmol, 11 mg) was dissolved in methanol (10 mL) and water (5 mL) and then added to the GO@ZIF-67 solution with vigorous stirring for 24 h at room temperature. The final product was separated by centrifugation, washed with methanol and water several times and dried at 60 °C. The preparation of GO@ZIF-67@Mn and GO@ZIF-67@Fe followed a similar procedure.

### 2.4. Electrochemical measurements

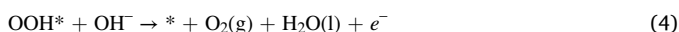
Electrochemical measurements of the acquired catalysts were conducted using an Autolab potentiostat within a three-electrode configuration immersed in a 1.0 M KOH solution. The standard three-electrode system consisted of glassy carbon (GC) as the working electrode, and platinum and Ag/AgCl as the counter and reference electrodes, respectively. To prepare the working electrode a slurry was formed by dispersing 3 mg of the catalyst and 5  $\mu$ L of Nafion solution (5%) in 500  $\mu$ L of ethanol, which was sonicated for 30 min to ensure uniformity. Subsequently, 5  $\mu$ L of the slurry was coated onto a pre-polished and cleaned glass carbon electrode (GCE) and dried at room temperature. Linear sweep voltammetry was performed at a scan rate of 5 mV s<sup>-1</sup>. To standardize the potentials, all measurements obtained using an Ag/AgCl electrode were converted to the potential reversible hydrogen electrode (RHE) scale using the equation  $E_{\text{RHE}} = E_{\text{Ag/AgCl}} + 0.059 \text{ pH} + E_{\text{Ag/AgCl}}^{\circ}$ , where  $E_{\text{Ag/AgCl}}$  denoted the measured potential and  $E_{\text{Ag/AgCl}}^{\circ} = 0.197$  V.

### 2.4. DFT calculations

All DFT calculations performed in this investigation were carried out using the Vienna ab initio simulation package (VASP) [43]. The Perdew-Burke-Ernzerhof (PBE) exchange-correlation functional of the generalized gradient approximation (GGA) was utilized to optimize structures, obtain free energetics of all the species and describe band structures [44]. The projector-augmented wave (PAW) potentials were used to describe the ionic cores and incorporate the contribution of valence electrons within the calculations [45]. The plane-wave basis function cutoff energy was set at 450 eV. A Monkhorst–Pack k-point net

of  $2 \times 2 \times 1$  was employed to sample the Brillouin zone. To model the systems,  $1 \times 1 \times 1$  supercells were built, and the slab models were constructed by slicing the plane (011) to represent the surface condition of the  $\text{Co}_6\text{C}_{72}\text{N}_{36}$  (ZIF-67) supercell. In addition, ZIF-67@Mn, ZIF-67@Fe and ZIF-67@MnFe were built by combining Fe and Mn atoms with ZIF-67. To eliminate interaction between supercells, a vacuum zone of 15 Å was added between two adjacent sheets. All atoms were allowed to relax during geometric optimization, with the convergence of total energy and force set at  $10^{-5}$  eV and 0.05 eV, respectively. Since the d electrons of Fe, Co, and Mn atoms exhibit strong Coulomb repulsion, the DFT +  $U$  method with  $U = 4.0$  eV was used for all transition metals [46].

In an alkaline environment, the energy profiles of the OER process can occur through a four-electron reaction mechanism, as represented by the following equations:



Here,  $*$  denotes the active sites on the surface,  $\text{O}^*$ ,  $\text{OOH}^*$ , and  $\text{OH}^*$  represent the adsorbed intermediates, and (g) and (l) represent the gas and liquid phases, respectively.

The Gibbs free energy change ( $\Delta G$ ) for each ORR/OER intermediate step can be calculated using the following equation:

$$\Delta G = \Delta E + \Delta ZPE - T\Delta S \quad (5)$$

Where  $\Delta E$ ,  $\Delta ZPE$ ,  $T$  and  $\Delta S$  refer to the DFT calculated reaction energy, the zero-point energy change, the temperature (298.15 K) and the entropy change, respectively [47].

The free energy difference for OER steps 1 through 4 can be calculated as follows:

$$\Delta G_1 = \Delta G_{\text{OH}^*} \quad (6)$$

$$\Delta G_2 = \Delta G_{\text{O}^*} - \Delta G_{\text{OH}^*} \quad (7)$$

$$\Delta G_3 = \Delta G_{\text{OOH}^*} - \Delta G_{\text{O}^*} \quad (8)$$

$$\Delta G_4 = 4.92 - \Delta G_{\text{OOH}^*} \quad (9)$$

The theoretical overpotential of a chemical reaction can be calculated by the following formula:

$$\eta = \max[\Delta G_1, \Delta G_2, \Delta G_3, \Delta G_4]/e - 1.23V \quad (10)$$

Since this formula is independent of pH, it applies to any condition.

### 3. Results and discussion

The morphology and structure of GO@ZIF-67@MnFe were investigated using SEM and TEM. The SEM images revealed uniform rhombic dodecahedral crystals of GO@ZIF-67@MnFe (Fig. 1a, b), which were also confirmed by TEM (Fig. 1c, d). Additionally, TEM images clearly showed the layered structure of GO and embedded Mn and Fe nanoparticles in GO@ZIF-67. Elemental mapping of GO@ZIF-67@MnFe using energy-dispersive X-ray (EDX) demonstrated a uniform distribution of C, N, O, Co, Mn, and Fe elements in the sample (Fig. 2a–g). Furthermore, the EDX analysis provided the molar ratio of all elements in GO@ZIF-67@MnFe (Fig. 2h), with the Mn:Fe ratio being almost 1:1. These findings demonstrate the successful synthesis of GO@ZIF-67@MnFe.

The crystal structure of GO@ZIF-67@MnFe, ZIF-67, and GO was identified by X-ray diffraction (XRD). The diffraction peaks at  $7.38^\circ$ ,  $10.43^\circ$ ,  $12.68^\circ$ ,  $14.78^\circ$ ,  $16.53^\circ$ ,  $18.08^\circ$ ,  $22.18^\circ$ ,  $24.53^\circ$ ,  $26.68^\circ$ ,  $29.68^\circ$ ,  $30.68^\circ$  and  $32.43^\circ$  were assigned to different crystalline planes of ZIF-

67, such as (011), (002), (112), (022), (013), (222), (114), (233), (134), (044), (244), and (235) (Fig. 3). The (001) plan of GO was identified at  $10.83^\circ$ . The peaks of GO@ZIF-67@MnFe confirmed the successful integration of ZIF-67 and GO, with a decrease in the intensity of ZIF-67 and GO peaks indicating the presence of Mn and Fe. These XRD results provide evidence of the successful formation of GO@ZIF-67@MnFe.

The XPS wide-scan spectra were utilized to corroborate the valence states of the constituent atoms in GO@ZIF-67@MnFe, and the binding energies of C, N, O, Co, Mn, and Fe were observed in the spectra. The C1s spectrum in Fig. 4 exhibited four distinct chemical functional groups: C-C/C = C bond (282.3 eV), C = N bond (283.1 eV), C-N/C = O bond (284.1 eV), and C-O bond (285.9 eV), indicating the presence of GO and ZIF-67 [48,49]. The high-resolution N 1 s spectrum displayed four peaks at 398.2 eV, 399.1 eV, 400.7 eV, and 402.1 eV, which corresponded to pyridinic, pyrrolic, graphitic N, and pyridinic  $N^{+}-O^-$ , respectively [50, 51]. Two groups of spin-orbit resolved peaks at 640.2 eV, 651.7 eV and 645.3 eV, 656.4 eV were observed and represented  $\text{Mn}^{2+}$   $2p_{3/2}$ ,  $\text{Mn}^{2+}$   $2p_{1/2}$  and  $\text{Mn}^{4+}$   $2p_{3/2}$ ,  $\text{Mn}^{4+}$   $2p_{1/2}$ , respectively [52,53]. The Fe 2p binding energy at 708.7 eV and 723.3 eV were attributed to  $\text{Fe}^{2+}$   $2p_{3/2}$  and  $\text{Fe}^{2+}$   $2p_{1/2}$ , while the peaks at 712.3 eV and 731.6 eV corresponded to  $\text{Fe}^{3+}$   $2p_{3/2}$  and  $\text{Fe}^{3+}$   $2p_{1/2}$ , respectively [54]. The Co 2p high-resolution XPS spectrum displayed peaks at 778.8 eV, 796.1 eV and 784.6 eV, 801.9 eV, which corresponds to  $\text{Co}^{2+}$   $2p_{3/2}$ ,  $\text{Co}^{2+}$   $2p_{1/2}$ , and  $\text{Co}^{3+}$   $2p_{3/2}$ ,  $\text{Co}^{3+}$   $2p_{1/2}$ , respectively [55,56].

### 3.1. Electrochemical performance for OER

To investigate the electrocatalytic activity and reaction kinetics of all catalysts, the OER was investigated by LSV curves at a scan rate of 5 mV s<sup>-1</sup> in 1.0 M KOH electrolyte. All LSV data were 100% IR-corrected manually using electrochemical impedance spectroscopy (EIS) analysis. Fig. 5a displays the OER polarization curves of GO@ZIF-67@MnFe, GO@ZIF-67@Mn, GO@ZIF-67@Fe, and GO@ZIF-67. GO@ZIF-67@MnFe exhibited a lower onset potential of 1.44 V when compared to GO@ZIF-67@Mn (1.48 V), GO@ZIF-67@Fe (1.54 V), and GO@ZIF-67 (1.62 V). The overpotentials of GO@ZIF-67@MnFe were calculated to be 236 and 380 mV at current densities of 10 and 100 mA cm<sup>-2</sup>, respectively. The electrocatalytic activity of GO@ZIF-67@MnFe was evaluated in comparison to the established commercial OER reference, RuO<sub>2</sub>, under standardized conditions. In Fig. S1, LSV curves obtained at a scan rate of 5 mV s<sup>-1</sup> in 1.0 M KOH electrolyte are shown. The results obtained indicate that GO@ZIF-67@MnFe exhibits significantly higher OER activity than RuO<sub>2</sub>. Additionally, the effect of the Fe:Mn molar ratio on the OER performance was assessed, and according to Fig. 5b, the overpotentials for GO@ZIF-67@MnFe with Fe:Mn molar ratios of 1:1, 1:2, and 2:1 were 236, 310, and 317 mV, respectively, at a current density of 10 mA cm<sup>-2</sup>. To further confirm the superiority of GO@ZIF-67@MnFe, its electrocatalytic activity was compared with ZIF-67@MnFe (Fig. 5c). The results indicate that the removal of GO from the catalyst increased the catalyst's overpotential, as the high surface and conductivity of GO as a result of the high oxygen sites and coordination with metals resulted in rapid electron transfer, increased current density and ultimately increased catalytic activity as a consequence [57–59]. Due to the interference of a tremendous number of gas bubbles released at high current densities, the cross-over between LSV curves at high current densities was observed.

Finally, it was observed that changing the oxidation states of Fe in the prepared catalyst revealed that  $\text{Fe}^{2+}$  exhibited higher catalytic activity than  $\text{Fe}^{3+}$  (Fig. 5d). In this case, the valence electron configuration of  $\text{Fe}^{2+}$  was characterized by a  $3d^6$  configuration, with four electron-filled  $t_{2g}$  orbitals and two electron-filled  $e_g$  orbitals. Conversely,  $\text{Fe}^{3+}$  exhibited a valence electron configuration of  $3d^5$ , with three electron-filled  $t_{2g}$  orbitals and two electron-filled  $e_g$  orbitals. Moreover,  $\text{Co}^{2+}$  possessed a valence electron configuration of  $3d^7$ , featuring a filled  $t_{2g}$  orbital and one electron-filled  $e_g$  orbital. The heightened electron



**Scheme 1.** Schematic illustration of the synthetic process for GO@ZIF-67@MnFe.

interaction stemming from the 3d electrons in the eg orbital of  $\text{Fe}^{2+}$ , which delocalized onto  $\text{Co}^{2+}$ , was observed. This electron delocalization phenomenon resulted in an increase in the valence state of  $\text{Fe}^{2+}$  (denoted as  $\delta$ ) and a concurrent decrease in the valence state of Co (denoted as  $\delta 1$ ). A novel electronic structure of  $\text{Fe}^{2+}$  reacted with adsorbed OH<sup>-</sup> and accelerates OER [60–62].

Electrochemical impedance spectroscopy (EIS) was employed for the characterization of the charge-transfer resistances ( $R_{ct}$ ) values of different samples. Fig. 6a illustrates that GO, ZIF-67, GO@ZIF-67 and GO@ZIF-67@MnFe had charge-transfer resistances ( $R_{ct}$ ) of 3035.58, 3394.24  $\Omega$ , 3830.48  $\Omega$ , and 250.1  $\Omega$ , respectively. The data indicate that GO@ZIF-67@MnFe exhibits faster electronic transfer rates and more exposed active sites than other species, suggesting that the developed nanocomposite catalyst has a much lower activation barrier, facilitating the overall OER process. This improvement can be attributed to the synergistic effect of MnFe nanoparticles and ZIF-67, which results in the provision of more active sites, enhancement of electrical conductivity, and facilitation of the diffusion of electrolyte ions [40,63,64].

To assess the long-term durability of the catalysts, a chronopotentiometry test was utilized. Fig. 6b illustrates the stability of GO@ZIF-67@MnFe at a potential of 1.5 V in 1.0 M KOH for 24 h. The result demonstrates that there was no change in the current density of  $8.95 \text{ mA cm}^{-2}$  after 24 h, indicating that GO@ZIF-67@MnFe exhibited excellent durability. In the first hour, the current density decreased due to charging a double layer, which represented the formation of first the deposition nuclei on the glassy carbon surface [65,66]. It was also found that no significant differences were observed between the fresh GO@ZIF-67@MnFe and the used GO@ZIF-67@MnFe in terms of surface morphology (Figs. S3 and S4).

To gain further insight into the OER catalytic kinetics, Tafel plots of GO@ZIF-67, GO@ZIF-67@Fe, GO@ZIF-67@Mn, and GO@ZIF-67@MnFe were presented in Fig. 6c. The Tafel slope of GO@ZIF-67@MnFe was  $55.7 \text{ mV dec}^{-1}$ , which is smaller than 77.3, 251, and  $370.8 \text{ mV dec}^{-1}$  of GO@ZIF-67@Mn, GO@ZIF-67@Fe, and GO@ZIF-67, respectively. These results indicate that GO@ZIF-67@MnFe exhibits the most effective OER performance kinetics. The electrochemical active

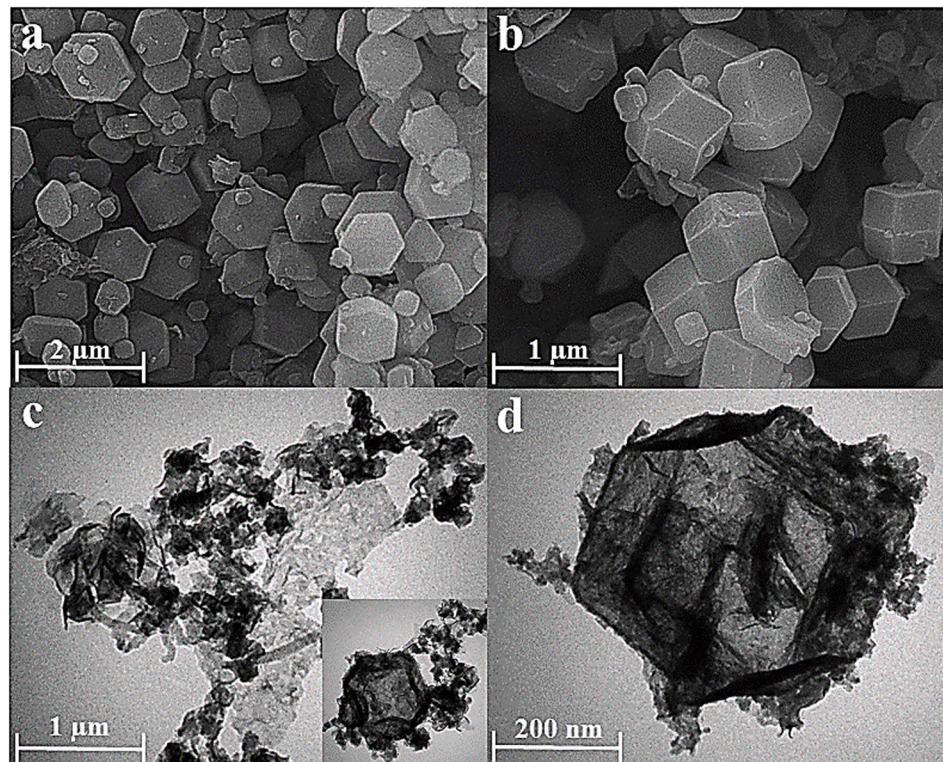


**Fig. 1.** Different-magnified SEM and TEM images of GO@ZIF-67@MnFe.

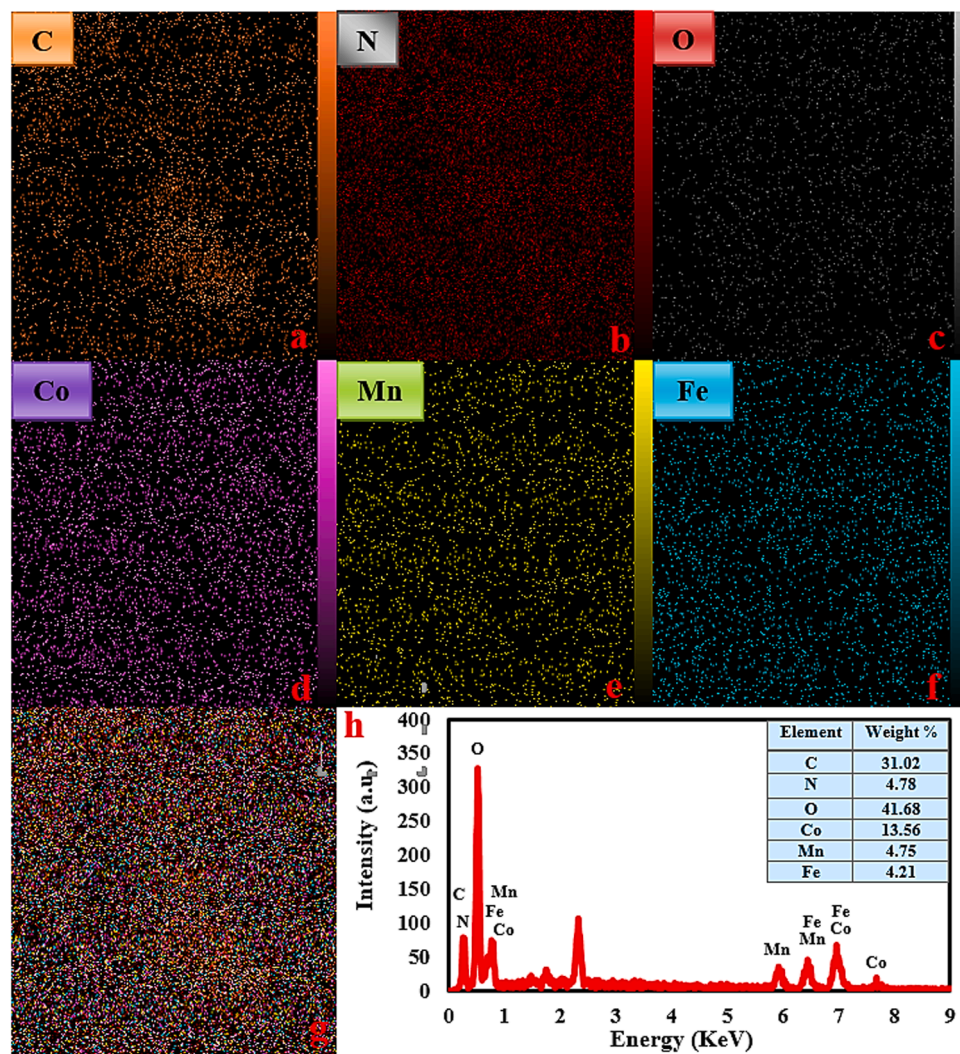


Fig. 2. EDX elemental mapping images and EDS spectrum of GO@ZIF-67@MnFe.

surface area (ECSA) was also examined in the non-faradaic region of the CV cycle by determining the electrochemical double-layer capacitance ( $C_{dl}$ ).  $C_{dl}$  was measured from the CV curves obtained at various scan rates at 20, 40, 60, 80 and 100 mV s<sup>-1</sup> (Fig. S2) within the potential range of 1.4–1.45 V, excluding redox processes. As shown in Fig. 6d, the GO@ZIF-67@MnFe has the highest  $C_{dl}$  value (123 mF cm<sup>-2</sup>) compared to GO@ZIF-67 (19.9 mF cm<sup>-2</sup>), ZIF-67@MnFe (6 mF cm<sup>-2</sup>), and ZIF-67 (5.4 mF cm<sup>-2</sup>), implying the presence of more no of electroactive sites in GO@ZIF-67@MnFe compared to other nanocomposites. It can be concluded that the high electroactive sites in GO@ZIF-67@MnFe caused a high level of OER activity.

To verify the structural stability of the catalyst after a long-term OER study, we performed a post-catalysis analysis, and the results are shown in Figs. S4 and S5. SEM images and EDX patterns, as shown in Figs. S4 and S5, indicate that structural features remain intact following OER.

The turn-over frequency (TOF) was calculated to investigate the intrinsic activity of all prepared catalysts at a potential of 1.5 V. To TOF calculation was used of the following equation:

$$TOF = \frac{j A}{4Fm}$$

Where  $j$  is the current density (mA cm<sup>-2</sup>),  $A$  is the geometrical surface area of the electrode (cm<sup>2</sup>),  $F$  is the Faraday constant (96,485 C mol<sup>-1</sup>), and  $m$  is the number of moles in the catalyst. The GO@ZIF-67@MnFe exhibited the highest TOF value of 0.0045 s<sup>-1</sup>, whereas

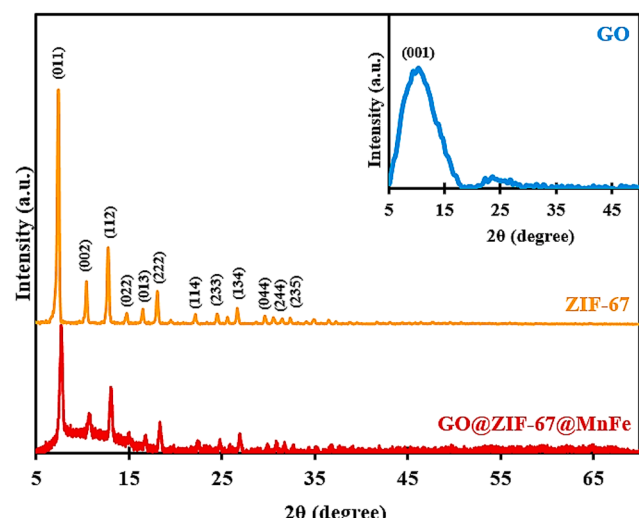


Fig. 3. XRD patterns of the ZIF-67 and as-prepared GO@ZIF-67@MnFe.

GO@ZIF-67@Mn, GO@ZIF-67@Fe and GO@ZIF-67 showed the TOF value of 0.0031, 0.0008 and 0.00012 s<sup>-1</sup>, respectively, confirming the outstanding intrinsic catalytic activity of GO@ZIF-67@MnFe to catalyze

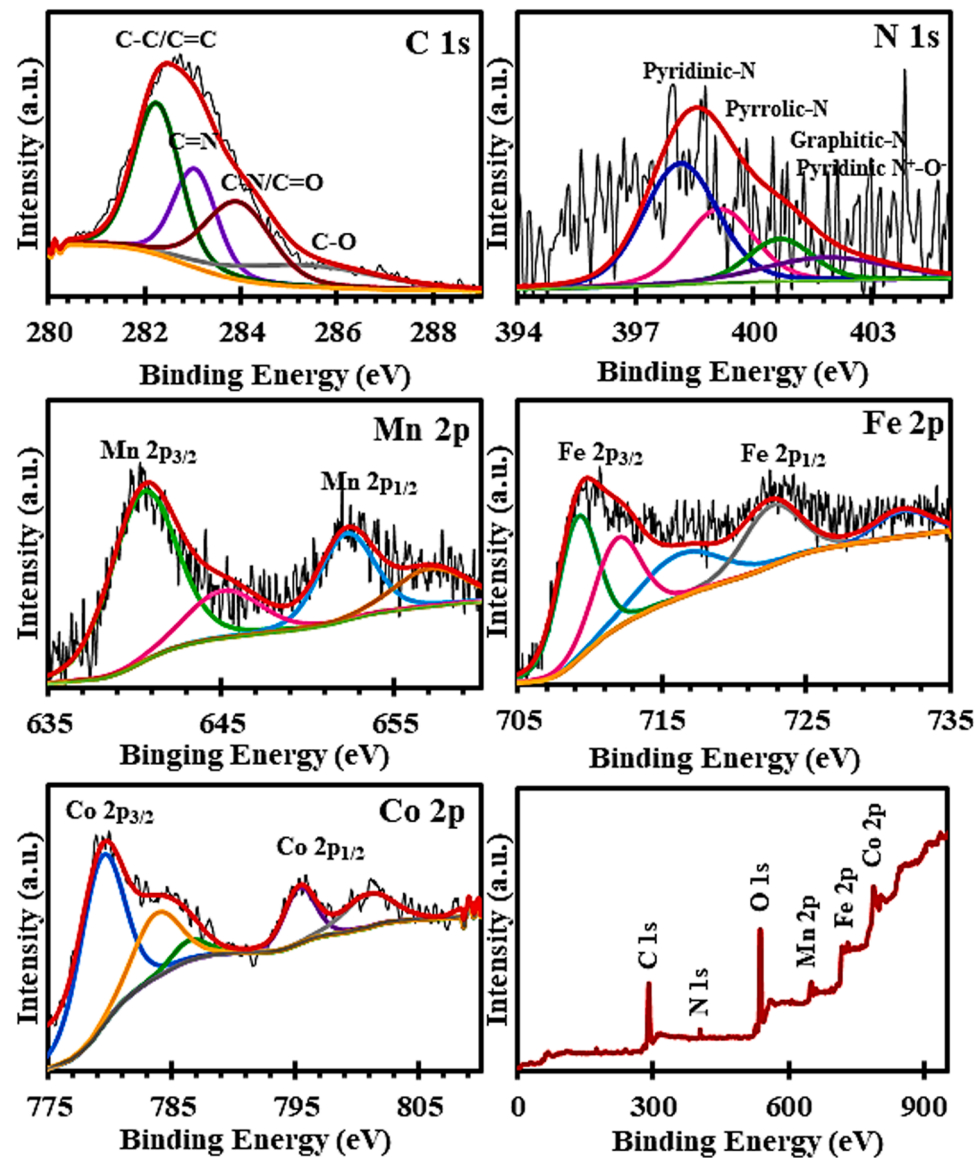
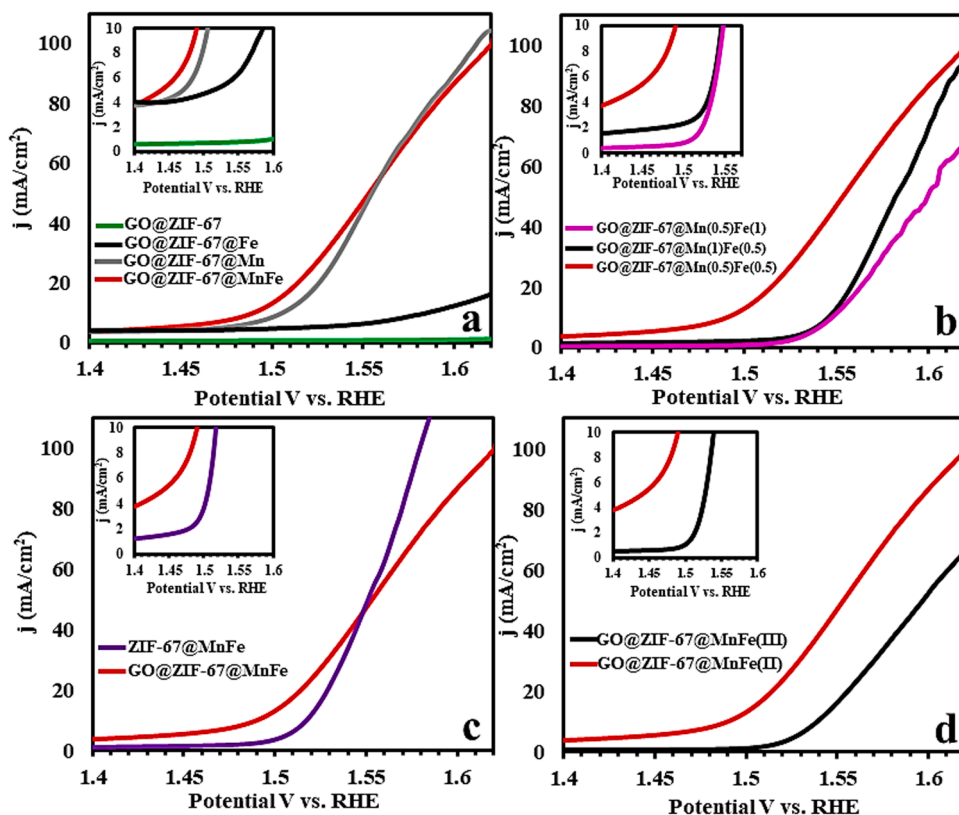


Fig. 4. XPS spectra of GO@ZIF-67@MnFe.



**Fig. 5.** OER polarization curves of (a) GO@ZIF-67@MnFe, GO@ZIF-67@Mn, GO@ZIF-67@Fe, GO@ZIF-67 (b) GO@ZIF-67@MnFe with molar ratios of Fe:Mn 1:1, 1:2 and 2:1 (c) GO@ZIF-67@MnFe and ZIF-67@MnFe, and (d) GO@ZIF-67@MnFe with varying oxidation states of Fe at a scan rate of 5 mV s<sup>-1</sup> in 1.0 M KOH electrolyte.

the OER reaction.

Besides, a comparison of the electrocatalytic performance of GO@ZIF-67@MnFe was made with other catalysts reported in Table 1, and the results indicated the superior electrochemical properties of GO@ZIF-67@MnFe. The high number of electrochemically active metallic sites on the surface and the low charge transfer resistance of GO@ZIF-67@MnFe led to better electrocatalytic performance and high electrochemical stability, which is the result of the effective combination of GO, ZIF-67, and MnFe. Accordingly, the GO@ZIF-67@MnFe catalyst with the lowest onset potential, overpotential, and Tafel slope showed higher OER performance than other catalysts of similar type.

### 3.2. Theoretical calculations

To better understand the mechanism of OER catalysis in trimetallic ZIFs compared to bimetallic and single metallic ZIFs, DFT calculations were used to determine the electronic structures and catalytic activities of the intermediate species involved in electrochemical OER. Four models were constructed for simulations, including Co<sub>6</sub>C<sub>72</sub>N<sub>36</sub> (ZIF-67), ZIF-67@Mn, ZIF-67@Fe and ZIF-67@MnFe (Fig. S5). The Gibbs free energies of four elementary reactions were calculated on the Cobalt active site for ZIF-67@Mn, ZIF-67@Fe and ZIF-67@MnFe. The reaction pathways of OH\*, O\*, and OOH\* intermediate species are shown in Fig. 7a for each elementary step of the OER on ZIF-67@MnFe. The Gibbs free energy of formation was computed for each elementary step of the four-electron reaction pathway, as shown in Fig. 7b. The rate-determining step (RDS) was determined based on the maximum change in  $\Delta G$  [81], with the formation of O\* found to be the RDS of OER

for all systems. The ZIF-67@Mn and ZIF-67@Fe exhibit a greater  $\Delta G_2$  value compared to ZIF-67@MnFe, with corresponding  $\Delta G_2$  values of 2.25, 2.48, and 2.33 eV for ZIF-67@MnFe, ZIF-67@Mn and ZIF-67@Fe, respectively. These calculations show that the conversion energy barrier for OH\* to O\* is reduced from ZIF-67@MnFe to ZIF-67@Mn and ZIF-67@Fe. The partial density of states (PDOS) analysis was also performed to obtain additional information regarding the electronic structure (Fig. S6). The PDOS analysis reveals that the d orbital of Cobalt in ZIF-67@MnFe has higher overlap with the p orbital of OH\* intermediate than ZIF-67@Mn and ZIF-67@Fe, indicating the better electrochemical performance of ZIF-67@MnFe than ZIF-67@Mn and ZIF-67@Fe [82,83]. These findings validate experimental results which demonstrate the superior performance of ZIF-67@MnFe over ZIF-67@Mn and ZIF-67@Fe.

### 4. Conclusions

In this study, a facile synthetic approach was used to obtain Fe and Mn embedded in the surface of ZIF-67 propagated on graphene oxide (GO@ZIF-67@MnFe). The resulting material exhibited excellent electrocatalytic activity for OER in alkaline electrolytes, requiring only overpotentials of 236 and 380 mV at current densities of 10 and 100 mA cm<sup>-2</sup>, respectively. The GO@ZIF-67@MnFe demonstrated higher electrocatalytic activity than GO@ZIF-67, GO@ZIF-67@Mn, GO@ZIF-67@Fe, and ZIF-67@MnFe, which was attributed to its specific architecture and the synergistic effect of the Co, Mn, and Fe species. Additionally, GO@ZIF-67@MnFe exhibited exceptional stability, maintaining a current density of 8.95 mA cm<sup>-2</sup> at a potential of 1.5 V for

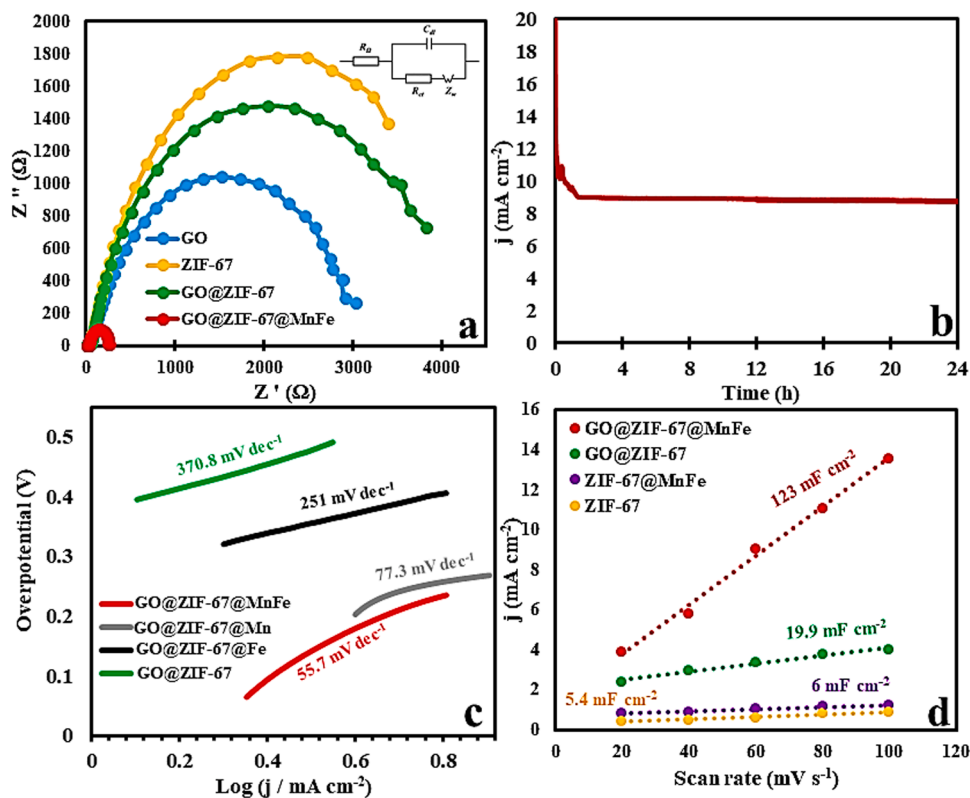


**Fig. 6.** (a) EIS Nyquist plots of GO@ZIF-67@MnFe for the OER conducted at a potential of 1.5 V (vs RHE) using corresponding equivalent circuits (inset), (b) Time-dependent current density curves of GO@ZIF-67@MnFe over of 24 h, (c) Tafel plots of GO@ZIF-67, GO@ZIF-67@Fe, GO@ZIF-67@Mn and GO@ZIF-67@MnFe, and (d) electrochemical double-layer capacitance (Cdl) of GO@ZIF-67@MnFe, GO@ZIF-67, ZIF-67@MnFe and ZIF-67.

**Table 1**  
Comparison of OER performance for the reported ZIF-67-based electrode materials and GO@ZIF-67@MnFe.

| Entry | Catalyst   | Onset (V)(10 mV cm <sup>-2</sup> ) | Tafel slope (mV dec <sup>-1</sup> ) | Overpotential (mV) (10 mV cm <sup>-2</sup> ) | Refs.     |
|-------|--|------------------------------------|-------------------------------------|--|-----------|
| 1     | Co <sub>3</sub> O <sub>4</sub> -CNTs                             | 1.62                               | 87                                  | 370  | [67]      |
| 2     | Co/Co <sub>4</sub> N@NC/rGO                                      | 1.622                              | 102.7                               | 372.1  | [68]      |
| 3     | MoS <sub>2</sub> @CoNi-ZIF(3–1)                                  | 1.55                               | 61                                  | 300  | [69]      |
| 4     | Co-Mo-N-PHP  | 1.54                               | 57                                  | 294  | [70]      |
| 5     | NiFeCo-LDH/CF  | 1.499                              | 42                                  | 249  | [71]      |
| 6     | Ni <sub>3</sub> Fe/Co-N-C  | 1.55                               | 53                                  | 310  | [72]      |
| 7     | MnCo <sub>2</sub> O <sub>4</sub> @Co <sub>3</sub> O <sub>4</sub> | 1.53                               | 109.6                               | 280  | [73]      |
| 8     | CoNC/Co@CC   | 1.61                               | 76.9                                | 361  | [24]      |
| 9     | FeCo <sub>1.11</sub> Te <sub>2</sub> @NCNTF-2                    | 1.61                               | 91                                  | 297  | [26]      |
| 10    | SiW <sub>x</sub> Co <sub>3</sub> [h]@ZIF-67                      | 1.65                               | 93.9                                | 420  | [74]      |
| 11    | N,S-Co@C   | 1.64                               | 101                                 | 410  | [75]      |
| 12    | SiW9Co3@ZIF-67   | 1.70                               | 113.6                               | 470  | [76]      |
| 13    | NiMn-ZIF-NF  | 1.48                               | 95                                  | 256  | [77]      |
| 14    | Co-M-Fe/Ni (150)   | 1.5                                | 50                                  | 269  | [78]      |
| 15    | ZIF-67@CNT   | 1.53                               | 98                                  | 285  | [79]      |
| 16    | Mn-ZIF-67-NF   | 1.5                                | 125                                 | 302  | [80]      |
| 17    | GO@ZIF-67@MnFe   | 1.466                              | 55.7                                | 236  | This Work |

24 h. Furthermore, DFT calculations confirmed the excellent electrocatalytic performance of the ZIFs. Overall, this study provides a promising approach to synthesizing OER electrocatalysts and inspires the development of ZIF derivatives for energy-related applications.

#### CRediT authorship contribution statement

**Zhwan Naghshbandi:** Writing – original draft, Data curation, Conceptualization. **Kayvan Moradi:** Writing – review & editing, Software, Investigation. **Abdollah Salimi:** Writing – review & editing, Supervision, Conceptualization. **Mohammad Gholinejad:** Supervision, Investigation. **Ali Feizabadi:** Writing – review & editing, Methodology, Investigation.

#### Declaration of competing interest

The authors declare that they have no known competing financial interests or personal relationships that could have appeared to influence the work reported in this paper.

#### Data availability

Data will be made available on request.

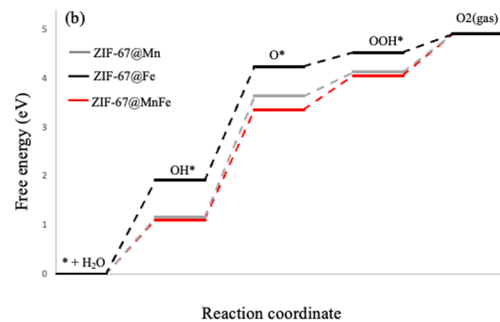
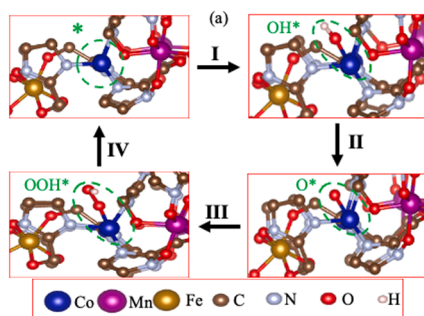


**Fig. 7.** DFT calculation for the OER on bimetallic and trimetallic ZIFs: (a) Elementary reaction steps of the OER process on the Co site with the intermediates ( $\text{OH}^*$ ,  $\text{O}^*$ ) in the structure of trimetallic ZIF. (b) Gibbs free energy diagrams of each reaction step in the OER process.

## Acknowledgements

This project was supported by Research Office of University of Kurdistan and Institute for Advanced Studies in Basic Sciences (IASBS) Zanjan-Iran. The financial support of Iranian Nanotechnology Initiative is also acknowledged. K. M expresses gratitude for the financial support received from the Academy of Finland for the CompEL, Finland project (#338228).

## Supplementary materials

Supplementary material associated with this article can be found, in the online version, at [doi:10.1016/j.electacta.2024.143884](https://doi.org/10.1016/j.electacta.2024.143884).

## References

- [1] Z.P. Wu, X.F. Lu, S.Q. Zang, X.W. Lou, Non-noble-metal-based electrocatalysts toward the oxygen evolution reaction, *Adv. Funct. Mater.* 30 (15) (2020) 1910274.
- [2] L. Tian, X. Zhai, X. Wang, J. Li, Z. Li, Advances in manganese-based oxides for oxygen evolution reaction, *J. Mater. Chem. B* 8 (29) (2020) 14400–14414.
- [3] Q. Shi, C. Zhu, D. Du, Y. Lin, Robust noble metal-based electrocatalysts for oxygen evolution reaction, *Chem. Soc. Rev.* 48 (12) (2019) 3181–3192.
- [4] J. Du, F. Li, L. Sun, Metal-organic frameworks and their derivatives as electrocatalysts for the oxygen evolution reaction, *Chem. Soc. Rev.* 50 (4) (2021) 2663–2695.
- [5] E. Fabbri, T.J. Schmidt, Oxygen Evolution Reaction—The Enigma in Water Electrolysis, ACS Publications, 2018, pp. 9765–9774.
- [6] C. Feng, M.B. Faheem, J. Fu, Y. Xiao, C. Li, Y. Li, Fe-based electrocatalysts for oxygen evolution reaction: progress and perspectives, *ACS Catal.* 10 (7) (2020) 4019–4047.
- [7] W. Zhou, D.D. Huang, Y.P. Wu, J. Zhao, T. Wu, J. Zhang, D.S. Li, C. Sun, P. Feng, X. Bu, Stable hierarchical bimetal-organic nanostructures as highperformance electrocatalysts for the oxygen evolution reaction, *Angew. Chem. Int. Ed.* 58 (13) (2019) 4227–4231.
- [8] P.P. Lopes, D.Y. Chung, X. Rui, H. Zheng, H. He, P. Farinazzo Bergamo Dias Martins, D. Strmcnik, V.R. Stamenovic, P. Zapol, J. Mitchell, Dynamically stable active sites from surface evolution of perovskite materials during the oxygen evolution reaction, *J. Am. Chem. Soc.* 143 (7) (2021) 2741–2750.
- [9] H. Xu, H. Shang, C. Wang, L. Jin, C. Chen, C. Wang, Y. Du, Three-dimensional open CoMoO<sub>x</sub>/CoMoS<sub>x</sub> nanobox electrocatalysts for efficient oxygen evolution reaction, *Appl. Catal. B* 265 (2020) 118605.
- [10] L. Bai, C.S. Hsu, D.T. Alexander, H.M. Chen, X. Hu, A cobalt–iron double-atom catalyst for the oxygen evolution reaction, *J. Am. Chem. Soc.* 141 (36) (2019) 14190–14199.
- [11] X. Xiao, C.T. He, S. Zhao, J. Li, W. Lin, Z. Yuan, Q. Zhang, S. Wang, L. Dai, D. Yu, A general approach to cobalt-based homobimetallic phosphide ultrathin nanosheets for highly efficient oxygen evolution in alkaline media, *Energy Environ. Sci.* 10 (4) (2017) 893–899.
- [12] Z. Li, H. He, H. Cao, S. Sun, W. Diao, D. Gao, P. Lu, S. Zhang, Z. Guo, M. Li, Atomic Co/Ni dual sites and Co/Ni alloy nanoparticles in N-doped porous Janus-like carbon frameworks for bifunctional oxygen electrocatalysis, *Appl. Catal. B* 240 (2019) 112–121.
- [13] Y. Li, T. Zhao, M. Lu, Y. Wu, Y. Xie, H. Xu, J. Gao, J. Yao, G. Qian, Q. Zhang, Enhancing oxygen evolution reaction through modulating electronic structure of trimetallic electrocatalysts derived from metal-organic frameworks, *Small* 15 (43) (2019) 1901940.
- [14] H. Rajan, M. Christy, V.R. Jothi, S. Anantharaj, S.C. Yi, A bifunctional hexafilamentous microfibril multimetallic foam: an unconventional high-performance electrode for total water splitting under industrial operation conditions, *J. Mater. Chem. B* 9 (8) (2021) 4971–4983.
- [15] Y. Zhang, W. Ye, J. Fan, V. Cecen, P. Shi, Y. Min, Q. Xu, Cobalt-nanoparticle-decorated cobalt–molybdenum bimetal oxides embedded in flower-like N-doped carbon as a durable and efficient electrocatalyst for oxygen evolution reaction, *ACS Sustain. Chem. Eng.* 9 (33) (2021) 11052–11061.
- [16] W. Ma, Q. Jiang, P. Yu, L. Yang, L. Mao, Zeolitic imidazolate framework-based electrochemical biosensor for *in vivo* electrochemical measurements, *Anal. Chem.* 85 (15) (2013) 7550–7557.
- [17] C. Duan, K. Liang, J. Lin, J. Li, L. Li, L. Kang, Y. Yu, H. Xi, Application of hierarchically porous metal-organic frameworks in heterogeneous catalysis: a review, *Sci. China Mater.* 65 (2) (2022) 298–320.
- [18] C. Adhikari, A. Das, A. Chakraborty, Zeolitic imidazole framework (ZIF) nanospheres for easy encapsulation and controlled release of an anticancer drug doxorubicin under different external stimuli: a way toward smart drug delivery system, *Mol. Pharm.* 12 (9) (2015) 3158–3166.
- [19] H. Zhang, J. Huo, H. Yang, F. Li, C. Duan, H. Xi, Green and rapid preparation of hierarchically porous metal-organic zeolites and simulation of their growth, *J. Mater. Chem. B* 7 (3) (2019) 1022–1029.
- [20] H. Chen, X. Wu, R. Zhao, Z. Zheng, Q. Yuan, Z. Dong, W. Gan, Preparation of reduced graphite oxide loaded with cobalt (II) and nitrogen co-doped carbon polyhedrons from a metal-organic framework (type ZIF-67), and its application to electrochemical determination of metronidazole, *Microchim. Acta* 186 (2019) 1–9.
- [21] Y. Liu, H. Pang, X. Wang, S. Yu, Z. Chen, P. Zhang, L. Chen, G. Song, N.S. Alharbi, S.O. Rabah, Zeolitic imidazolate framework-based nanomaterials for the capture of heavy metal ions and radionuclides: a review, *J. Chem. Eng.* 406 (2021) 127139.
- [22] Y. Liu, H. Cheng, M. Cheng, Z. Liu, D. Huang, G. Zhang, B. Shao, Q. Liang, S. Luo, T. Wu, The application of Zeolitic imidazolate frameworks (ZIFs) and their derivatives based materials for photocatalytic hydrogen evolution and pollutants treatment, *J. Chem. Eng.* 417 (2021) 127914.
- [23] G. Zhong, D. Liu, J. Zhang, The application of ZIF-67 and its derivatives: adsorption, separation, electrochemistry and catalysts, *J. Mater. Chem. B* 6 (5) (2018) 1887–1899.
- [24] H. Wen, S. Zhang, T. Yu, Z. Yi, R. Guo, ZIF-67-based catalysts for oxygen evolution reaction, *Nanoscale* 13 (28) (2021) 12058–12087.
- [25] A.M. Mohamed, M. Ramadan, N.K. Allam, Recent advances on zeolitic imidazolate-67 metal-organic framework-derived electrode materials for electrochemical supercapacitors, *J. Energy Storage* 34 (2021) 102195.
- [26] X. Yang, J. Chen, Y. Chen, P. Feng, H. Lai, J. Li, X. Luo, Novel Co 3 O 4 nanoparticles/nitrogen-doped carbon composites with extraordinary catalytic activity for oxygen evolution reaction (OER), *Nano-Micro Lett.* 10 (2018) 1–11.
- [27] W. Yang, Y. Bai, J. Ma, Z. Wang, W. Sun, J. Qiao, H. Cai, K. Sun, Engineering of carbon nanotube-grafted carbon nanosheets encapsulating cobalt nanoparticles for efficient electrocatalytic oxygen evolution, *J. Mater. Chem. B* 8 (47) (2020) 25268–25274.
- [28] J. Ren, X. Yang, J. Yu, X. Wang, Y. Lou, J. Chen, A MOF derived Co-NC@CNT composite with a 3D interconnected conductive carbon network as a highly efficient cathode catalyst for Li-O<sub>2</sub> batteries, *Sustain. Energy Fuels* 4 (12) (2020) 6105–6111.
- [29] G. Wang, X. Chen, S. Liu, C. Wong, S. Chu, Mechanical chameleon through dynamic real-time plasmonic tuning, *ACS Nano* 10 (2) (2016) 1788–1794.
- [30] Y. Tan, Z. Zhang, Z. Lei, W. Wu, W. Zhu, N. Cheng, S. Mu, Thiourea-Zeolitic imidazolate Framework-67 assembly derived Co-CoO nanoparticles encapsulated in N, S Codoped open carbon shell as bifunctional oxygen electrocatalyst for rechargeable flexible solid Zn–Air batteries, *J. Power Sources* 473 (2020) 228570.
- [31] B. He, X.C. Wang, L.X. Xia, Y.Q. Guo, Y.W. Tang, Y. Zhao, Q.L. Hao, T. Yu, H.K. Liu, Z. Su, Metal-organic framework-derived Fe-doped Co<sub>1.11</sub>Te<sub>2</sub> embedded in nitrogen-doped carbon nanotube for water splitting, *ChemSusChem* 13 (19) (2020) 5239–5247.
- [32] X. Li, C. Xiao, X. Ruan, Y. Hu, C. Zhang, J. Cheng, Y. Chen, Enrofloxacin degradation in a heterogeneous electro-Fenton system using a tri-metal-carbon nanofibers composite cathode, *J. Chem. Eng.* 427 (2022) 130927.
- [33] J. Wang, C. Chen, N. Cai, M. Wang, H. Li, F. Yu, High topological tri-metal phosphide of Co@P FeNiP toward enhanced activities in oxygen evolution reaction, *Nanoscale* 13 (2) (2021) 1354–1363.
- [34] W. Zhao, N. Wu, F. Yu, B. Zhou, X. Chu, Z. Wei, S. Yang, Ultrathin, porous CoPS nanosheets: GO self-sacrificing template synthesis as bifunctional catalysts for overall water splitting, *ACS Appl. Energy Mater.* 4 (10) (2021) 10976–10985.

- [35] A. Mohammadi, N. Arsalani, A.G. Tabrizi, S.E. Moosavifard, Z. Naqshbandi, L. S. Ghadimi, Engineering rGO-CNT wrapped Co<sub>3</sub>S<sub>4</sub> nanocomposites for high-performance asymmetric supercapacitors, *J. Chem. Eng. Eng.* 334 (2018) 66–80.
- [36] Y. Tian, Z. Yu, L. Cao, X.L. Zhang, C. Sun, D.W. Wang, Graphene oxide: an emerging electromaterial for energy storage and conversion, *J. Energy Chem.* 55 (2021) 323–344.
- [37] D. Bahari, B. Babamiri, K. Moradi, A. Salimi, R. Hallaj, Graphdiyne nanosheet as a novel sensing platform for self-enhanced electrochemiluminescence of MOF enriched ruthenium (II) in the presence of dual co-reactants for detection of tumor marker, *Biosens. Bioelectron.* 195 (2022) 113657.
- [38] B. Cai, S. Wang, L. Huang, Y. Ning, Z. Zhang, G.J. Zhang, Ultrasensitive label-free detection of PNA-DNA hybridization by reduced graphene oxide field-effect transistor biosensor, *ACS Nano* 8 (3) (2014) 2632–2638.
- [39] K. Ji, X. Zhang, Q. Che, Y. Yue, P. Yang, Composite nanoarchitectonics of ZIF-67 derived CoSe<sub>2</sub>/rGO with superior charge transfer for oxygen evolution reaction, *Electrochim. Acta* 426 (2022) 140785.
- [40] W. Fang, J. Wang, Y. Hu, X. Cui, R. Zhu, Y. Zhang, C. Yue, J. Dang, W. Cui, H. Zhao, Metal-organic framework derived Fe-Co-CN/reduced graphene oxide for efficient HER and OER, *Electrochim. Acta* 365 (2021) 137384.
- [41] S.S. Sankar, G. Keerthana, K. Manjula, J.H. Sharad, S. Kundu, Electrospun Fe-incorporated ZIF-67 nanofibers for effective electrocatalytic water splitting, *Inorg. Chem.* 60 (2021) 4034–4046.
- [42] D.C. Marcano, D.V. Kosynkin, J.M. Berlin, A. Sinitskii, Z. Sun, A. Slesarev, L. B. Alemany, W. Lu, J.M. Tour, Improved synthesis of graphene oxide, *ACS Nano* 4 (8) (2010) 4806–4814.
- [43] G. Kresse, J. Furthmüller, Efficiency of ab-initio total energy calculations for metals and semiconductors using a plane-wave basis set, *Comput. Mater. Sci.* 6 (1) (1996) 15–50.
- [44] P. Perdew, K. Burke, M. Ernzerhof, Generalized gradient approximation made simple, *Phys. Rev. Lett.* 77 (18) (1996) 3865.
- [45] P.E. Blöchl, O. Jepsen, O.K. Andersen, Improved tetrahedron method for Brillouin-zone integrations, *Phys. Rev. B* 49 (23) (1994) 16223.
- [46] X.L. Wang, L.Z. Dong, M. Qiao, Y.J. Tang, J. Liu, Y. Li, S.L. Li, J.X. Su, Y.Q. Lan, Exploring the performance improvement of the oxygen evolution reaction in a stable bimetal-organic framework system, *Angew. Chem. Int. Ed.* 57 (31) (2018) 9660–9664.
- [47] J.K. Nørskov, J. Rossmeisl, A. Logadottir, L. Lindqvist, J.R. Kitchin, T. Bligaard, H. Jonsson, Origin of the overpotential for oxygen reduction at a fuel-cell cathode, *J. Phys. Chem. B* 108 (46) (2004) 17886–17892.
- [48] T.A. Makhetha, S.C. Ray, R.M. Moutlooi, Zeolitic imidazolate framework-8-encapsulated nanoparticle of ag/cu composites supported on graphene oxide: synthesis and antibacterial activity, *ACS Omega* 5 (17) (2020) 9626–9640.
- [49] Y. Zhang, Y.Q. Liu, W. Chu, Y. Bai, ZIF-8-derived N-doped porous carbon coated reduced graphene oxide as ultrasensitive platform and its application for electrochemical sensing, *J. Alloys Compd.* 857 (2021) 157604.
- [50] J. Xiong, X. Chen, Y. Zhang, Y. Lu, X. Liu, Y. Zheng, Y. Zhang, J. Lin, Fe/Co/N-C/graphene derived from Fe/ZIF-67/graphene oxide three dimensional frameworks as a remarkably efficient and stable catalyst for the oxygen reduction reaction, *RSC Adv.* 12 (4) (2022) 2425–2435.
- [51] H. Chen, X. Wu, R. Zhao, Z. Zheng, Q. Yuan, Z. Dong, W. Gan, Preparation of reduced graphite oxide loaded with cobalt (II) and nitrogen co-doped carbon polyhedrons from a metal-organic framework (type ZIF-67), and its application to electrochemical determination of metronidazole, *Microchim. Acta* 186 (2019) 1–9.
- [52] N. Liu, S. Shang, D. Shi, Q. Cheng, Z. Pan, Construction of hollow ZnO/Mn-ZIF-67 heterojunction photocatalysts: enhanced photocatalytic performance and mechanistic insight, *New J. Chem.* 45 (4) (2021) 2285–2294.
- [53] C. Jiao, Z. Wang, X. Zhao, H. Wang, J. Wang, R. Yu, D. Wang, Triple-shelled manganese–cobalt oxide hollow dodecahedra with highly enhanced performance for rechargeable alkaline batteries, *Angew. Chem. Int. Ed.* 58 (4) (2019) 996–1001.
- [54] L. Yang, Z. Shao, Tunable and convenient synthesis of highly dispersed Fe-N x catalysts from graphene-supported Zn-Fe-ZIF for efficient oxygen reduction in acidic media, *RSC Adv.* 9 (72) (2019) 42236–42244.
- [55] M. Zhao, A. Tesfay Reda, D. Zhang, Reduced graphene oxide/ZIF-67 aerogel composite material for uranium adsorption in aqueous solutions, *ACS Omega* 5 (14) (2020) 8012–8022.
- [56] M. Gholnejad, Z. Naghshbandi, J.M. Sansano, Zeolitic imidazolate frameworks-67 (ZIF-67) supported PdCu nanoparticles for enhanced catalytic activity in Sonogashira-Hagihara and nitro group reduction under mild conditions, *Mol. Catal.* 518 (2022) 112093.
- [57] Y. Gu, S. Chen, J. Ren, Y.A. Jia, C. Chen, S. Komarneni, D. Yang, X. Yao, Electronic structure tuning in Ni3FeN/r-GO aerogel toward bifunctional electrocatalyst for overall water splitting, *ACS Nano* 12 (2018) 245–253.
- [58] M. Jahan, Z. Liu, K.P. Loh, A Graphene oxide and copper-centered metal organic framework composite as a tri-functional catalyst for HER, OER, and ORR, *Adv. Funct. Mater.* 23 (2013) 5363–5372.
- [59] K. Lellala, Microwave-assisted facile hydrothermal synthesis of Fe3O4-GO nanocomposites for the efficient bifunctional electrocatalytic activity of OER/ORR, *Energy Fuels* 35 (2021) 8263–8274.
- [60] Y. Guo, G. Yan, X. Sun, S. Wang, L. Chen, Y. Feng, d-electron interactions induced CoV 2 O 6-Fe-NF for efficient oxygen evolution reaction, *RSC Adv.* 13 (2023) 18488–18495.
- [61] S.I. Bokarev, M. Dantz, E. Suljoti, O. Kühn, E.F. Aziz, State-dependent electron delocalization dynamics at the solute-solvent interface: soft-x-ray absorption spectroscopy and ab initio calculations, *Phys. Rev. Lett.* 111 (2013) 083002.
- [62] C. Chen, M. Sun, F. Zhang, H. Li, M. Sun, P. Fang, T. Song, W. Chen, J. Dong, B. Rosen, Adjacent Fe Site boosts electrocatalytic oxygen evolution at Co site in single-atom-catalyst through a dual-metal-site design, *Energy Environ. Sci.* 16 (2023) 1685–1696.
- [63] X. Chen, D. Liu, G. Cao, Y. Tang, C. Wu, *In situ* synthesis of a sandwich-like graphene@ ZIF-67 heterostructure for highly sensitive nonenzymatic glucose sensing in human serums, *ACS Appl. Mater. Interfaces* 11 (2019) 9374–9384.
- [64] F. Asadi, S.N. Azizi, S. Ghasemi, Preparation of Ag nanoparticles on nano cobalt-based metal organic framework (ZIF-67) as catalyst support for electrochemical determination of hydrazine, *J. Mater. Sci. Mater. Electron.* 30 (2019) 5410–5420.
- [65] S. Esmailzadeh, T. Shahrabi, Y. Yaghoubinezhad, G.B. Darband, An analytical study on nucleation and growth mechanism of nanostructured Ni-Se coating by the chronoamperometry and pulse potential techniques, *J. Electroanal. Chem.* 881 (2021) 114949.
- [66] M. Verma, L. Sinha, P.M. Shirage, Electrodeposited nanostructured flakes of cobalt, manganese and nickel-based sulfide (CoMnNiS) for electrocatalytic alkaline oxygen evolution reaction (OER), *J. Mater. Sci. Mater. Electron.* 32 (2021) 12292–12307.
- [67] J. Shen, J. Gao, L. Ji, X. Chen, C. Wu, Three-dimensional interlinked Co3O4-CNTs hybrids as novel oxygen electrocatalyst, *Appl. Surf. Sci.* 497 (2019) 143818.
- [68] H. Qi, Y. Feng, Z. Chi, Y. Cui, M. Wang, J. Liu, Z. Guo, L. Wang, S. Feng, *In situ* encapsulation of Co-based nanoparticles into nitrogen-doped carbon nanotubes-modified reduced graphene oxide as an air cathode for high-performance Zn-air batteries, *Nanoscale* 11 (45) (2019) 21943–21952.
- [69] Y. Liu, B. Hu, S. Wu, M. Wang, Z. Zhang, B. Cui, L. He, M. Du, Hierarchical nanocomposite electrocatalyst of bimetallic zeolitic imidazolate framework and MoS<sub>2</sub> sheets for non-Pt methanol oxidation and water splitting, *Appl. Catal. B* 258 (2019) 117970.
- [70] H. Chu, D. Zhang, B. Jin, M. Yang, Impact of morphology on the oxygen evolution reaction of 3D hollow cobalt-molybdenum nitride, *Appl. Catal. B* 255 (2019) 117744.
- [71] Y. Lin, H. Wang, C.K. Peng, L. Bu, C.L. Chiang, K. Tian, Y. Zhao, J. Zhao, Y.G. Lin, J. M. Lee, Co-induced electronic optimization of hierarchical NiFe LDH for oxygen evolution, *Small* 16 (38) (2020) 2002426.
- [72] J. Tan, T. Thomas, J. Liu, L. Yang, L. Pan, R. Cao, H. Shen, J. Wang, J. Liu, M. Yang, Rapid microwave-assisted preparation of high-performance bifunctional Ni3Fe/Co-NC for rechargeable Zn-air battery, *J. Chem. Eng.* 395 (2020) 125151.
- [73] J.J. Zhou, X. Han, K. Tao, Q. Li, Y.L. Li, C. Chen, L. Han, Shish-kebab type MnCo2O4@ Co3O4 nanoneedle arrays derived from MnCo-LDH@ ZIF-67 for high-performance supercapacitors and efficient oxygen evolution reaction, *J. Chem. Eng.* 354 (2018) 875–884.
- [74] V.K. Abdelkader-Fernández, D.M. Fernandes, S.S. Balula, L. Cunha-Silva, C. Freire, Advanced framework-modified POM@ ZIF-67 nanocomposites as enhanced oxygen evolution reaction electrocatalysts, *J. Mater. Chem. A* 8 (2020) 13509–13521.
- [75] V.K. Abdelkader-Fernandez, D.M. Fernandes, S.S. Balula, L. Cunha-Silva, M. J. Pérez-Mendoza, F.J. Lopez-Garzon, M.F. Pereira, C. Freire, Noble-metal-free MOF-74-derived nanocarbons: insights on metal composition and doping effects on the electrocatalytic activity toward oxygen reactions, *ACS Appl. Energy Mater.* 2 (2019) 1854–1867.
- [76] V.K. Abdelkader-Fernandez, D.M. Fernandes, S.S. Balula, L. Cunha-Silva, C. Freire, Oxygen evolution reaction electrocatalytic improvement in POM@ ZIF nanocomposites: a bidirectional synergistic effect, *ACS Appl. Energy Mater.* 3 (2020) 2925–2934.
- [77] S.S. Selvasundarasekar, S. Mahendran, R. Raj Mohamed, A. BaQais, M.A. Amin, S. Kundu, Boosting the activity of the oxygen evolution reaction through an electrospun nickel manganese-based bimetallic zeolite imidazolate framework fibrous system in alkaline medium, *Inorg. Chem.* 62 (2023) 6411–6420.
- [78] P. Chen, X. Duan, G. Li, X. Qiu, S. Wang, Y. Huang, A. Stavitskaya, H. Jiang, Construction of ZIF-67/MIL-88 (Fe, Ni) catalysts as a novel platform for efficient overall water splitting, *Int. J. Hydrog. Energy* 48 (2023) 7170–7180.
- [79] H.B. Jung, Y. Kim, J. Lim, S. Cho, M. Seo, I.S. Kim, M. Kim, C. Lee, Y.W. Lee, C. Y. Yoo, ZIF-67 metal-organic frameworks synthesized onto CNT supports for oxygen evolution reaction in alkaline water electrolysis, *Electrochim. Acta* 439 (2023) 141593.
- [80] S.S. Selvasundarasekar, T. Bijoy, S. Kumaravel, A. Karmakar, R. Madhu, K. Bera, S. Nagappan, H.N. Dhandapani, G.A. Mersal, M.M. Ibrahim, Effective formation of a Mn-ZIF-67 nanofibrous network via electrospinning: an active electrocatalyst for OER in alkaline medium, *ACS Appl. Mater. Interfaces* 14 (2022) 46581–46594.
- [81] L. Peng, J. Wang, Y. Nie, X. Xiong, Y. Wang, L. Zhang, K. Chen, W. Ding, L. Li, Z. Wei, Dual-ligand synergistic modulation: a satisfactory strategy for simultaneously improving the activity and stability of oxygen evolution electrocatalysts, *ACS Catal.* 7 (12) (2017) 8184–8191.
- [82] Y.T. Xu, Z.M. Ye, J.W. Ye, L.M. Cao, R.K. Huang, J.X. Wu, D.D. Zhou, X.F. Zhang, C. T. He, J.P. Zhang, Non-3d metal modulation of a cobalt imidazolate framework for excellent electrocatalytic oxygen evolution in neutral media, *Angew. Chem. Int. Ed.* 58 (1) (2019) 139–143.
- [83] W.H. Li, J. Lv, Q. Li, J. Xie, N. Ogiwara, Y. Huang, H. Jiang, H. Kitagawa, G. Xu, Y. Wang, Conductive metal-organic framework nanowire arrays for electrocatalytic oxygen evolution, *J. Mater. Chem. B* 7 (17) (2019) 10431–10438.